AGU PUBLICATIONS

JGR

Journal of Geophysical Research: Biogeosciences

RESEARCH ARTICLE
10.1002/2017JG003943

Key Points:
- Aerobic respiration and denitrification rates in beach aquifer intertidal circulation cells are heterogeneous
- Aerobic respiration is greatest along the landward freshwater-seawater mixing zone, while denitrification is greatest throughout the mixing zone
- Numerical simulations support field evidence of enhanced denitrification in the freshwater-seawater mixing zone of the circulation cell

Supporting Information:
- Supporting Information S1

Correspondence to:
H. A. Michael,
hmichael@udel.edu

Citation:
Kim, K. H., Heiss, J. W., Michael, H. A., Cai, W.-J., Laattoe, T., Post, V. E. A., & Ullman, W. J. (2017). Spatial patterns of groundwater biogeochemical reactivity in an intertidal beach aquifer. *Journal of Geophysical Research: Biogeosciences*, *122*. https://doi.org/10.1002/2017JG003943

Received 17 MAY 2017
Accepted 25 AUG 2017
Accepted article online 11 SEP 2017

Spatial Patterns of Groundwater Biogeochemical Reactivity in an Intertidal Beach Aquifer

Kyra H. Kim[1,2], James W. Heiss[1], Holly A. Michael[1,3], Wei-Jun Cai[2], Tariq Laattoe[4], Vincent E. A. Post[4], and William J. Ullman[2]

[1]Department of Geological Sciences, University of Delaware, Lewes, DE, USA, [2]School of Marine Science and Policy, University of Delaware, Newark, DE, USA, [3]Department of Civil and Environmental Engineering, University of Delaware, Newark, DE, USA, [4]School of the Environment, Flinders University, Newark, DE, USA

Abstract Beach aquifers host a dynamic and reactive mixing zone between fresh and saline groundwater of contrasting origin and composition. Seawater, driven up the beachface by waves and tides, infiltrates into the aquifer and meets the seaward-discharging fresh groundwater, creating and maintaining a reactive intertidal circulation cell. Within the cell, land-derived nutrients delivered by fresh groundwater are transformed or attenuated. We investigated this process by collecting pore water samples from multilevel wells along a shore-perpendicular transect on a beach near Cape Henlopen, Delaware, and analyzing solute and particulate concentrations. Pore water incubation experiments were conducted to determine rates of oxygen consumption and nitrogen gas production. A numerical model was employed to support field and laboratory interpretations. Results showed that chemically sensitive parameters such as pH and ORP diverged from salinity distribution patterns, indicating biogeochemical reactivity within the circulation cell. The highest respiration rates were found in the landward freshwater-saltwater mixing zone, supported by high dissolved inorganic carbon. Chlorophyll *a*, a proxy for phytoplankton, and particulate carbon did not co-occur with the highest respiration rates but were heterogeneously distributed in deeper and hypoxic areas of the cell. The highest rates of N_2 production were also found in the mixing zone coinciding with elevated O_2 consumption rates but closer to the lower discharge point. Model results were consistent with these observations, showing heightened denitrification in the mixing zone. The results of this work emphasize the relationship between the physical flow processes of the circulation cell and its biogeochemical reactivity and highlight the environmental significance of sandy beaches.

1. Introduction

Submarine groundwater discharge (SGD) is the flow of fresh or saline groundwater from the coastal aquifer to the adjacent marine surface water. SGD is an important pathway for the delivery of terrestrial solutes to coastal waters and can significantly impact marine ecosystems, as it generally contains higher concentrations of nutrients and other land-derived contaminants than surface water discharge (Johannes, 1980; Moore, 1999; Slomp & Van Cappellen, 2004).

Fresh coastal groundwater is driven seaward by an inland hydraulic gradient, while density gradients along the lower Ghyben-Herzberg interface create convective seawater circulation that contributes a portion of saline SGD (Figure 1) (Cooper, 1959; Kohout, 1960). In some beaches, a smaller, but chemically significant, intertidal cell of rapidly circulating saline water occurs landward of the zone of fresh SGD (Beck et al., 2017; Heiss & Michael, 2014; Michael et al., 2005; M. Robinson et al., 1998; C. Robinson et al., 2007; Seidel et al., 2015). Through tide and wave action, seawater moves up the beachface and infiltrates into the sand, where it circulates and mixes with the seaward moving fresh groundwater. Although the transition zone below this circulation cell is smaller than the Ghyben-Herzberg transition zone at depth, it can alter the distribution of solutes and solute fluxes.

Traditionally, quartz-rich beach sediments have been thought to be mostly unreactive due to their low organic matter content (Anschutz et al., 2009; Boudreau et al., 2001). However, the intertidal circulation cell has been shown to host various biogeochemical reactions that transform and attenuate land-derived nutrients prior to discharge, including oxic respiration of carbon (Beck et al., 2017; Charbonnier et al., 2013, Reckhardt et al., 2015; Seidel et al., 2015), nitrogen transformations (Hays & Ullman, 2007a, 2007b; Ullman et al., 2003), Fe oxidation and reduction (Charette & Sholkovitz, 2002; McAllister et al., 2015), other metal cycling processes (Reckhardt et al., 2015), and sorption. It is hypothesized that introduction of reactive

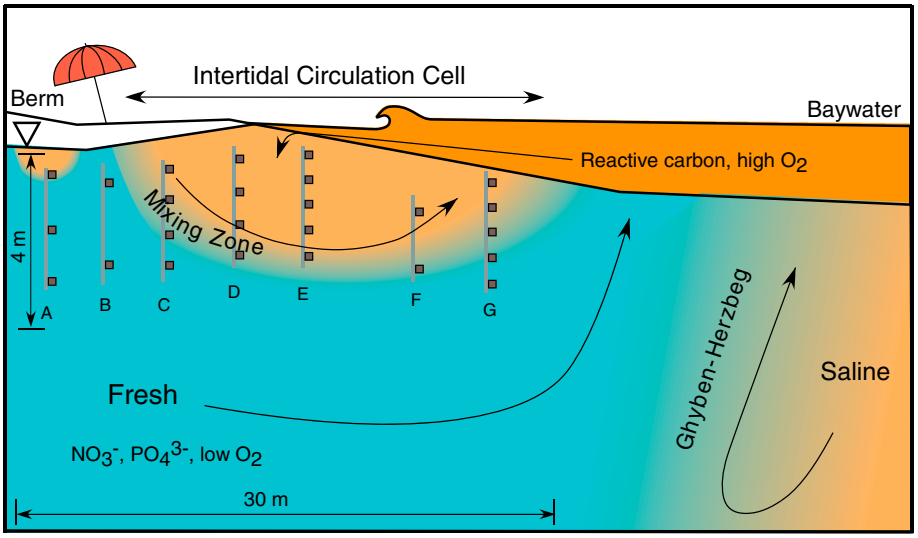

Figure 1. Schematic diagram of the intertidal circulation cell and the positions of multilevel pore water samplers (A–G) at Cape Shores. Each gray line indicates location of sampler and dark gray boxes indicate the approximate position and spacing of water sampling ports. Infiltration of saline seawater into the fresh groundwater creates a reactive intertidal circulation cell. Biogeochemical activity within this cell is supported by reactive organic carbon and oxygen originating from the infiltrating seawater.

organic matter and oxygen with infiltrating seawater into the intertidal circulation cell supports biogeochemical reactions with a variety of environmentally available electron acceptors (Charbonnier et al., 2013; Reckhardt et al., 2015; Seidel et al., 2015). This has substantial implications for coastal systems, as reactions hosted in the cell can alter the chemical characteristics of discharging waters, impacting coastal organisms and ecology (Anschutz et al., 2009; Burnett et al., 2003).

The intertidal circulation cell is highly dynamic and has been shown to respond to hydrologic, geologic, and topographic changes over various time scales (waves, tides, and seasons) (Bakhtyar et al., 2013; Heiss & Michael, 2014; M. Robinson et al., 1998; C. Robinson et al., 2006, 2007). Therefore, the flow paths that control the delivery and availability of reactive particles and solutes into the circulation cell are also both spatially and temporally variable. As the driving forces and physical characteristics of the cell change, the extent and patterns of chemical reactions within and around the cell are expected to respond in concert. While the dynamic nature of the physical properties of the cell has been described in detail (Heiss & Michael, 2014; Michael et al., 2005; M. Robinson et al., 1998; C. Robinson et al., 2007), there are fewer observations concerning the location and relative rates of chemical reactivity within the cell and their relations to the patterns of mixing.

Previous field studies have established the reactive nature of the intertidal circulation cell based on the surficial or cross-sectional distribution of solutes. Charbonnier et al. (2013) monitored solute concentrations across the water table at Truc Vert, France, and demonstrated enhanced, but seasonally variable, aerobic respiration in the lower beach. Reckhardt et al. (2015) observed the circulation cell across different hydrodynamic forcing regimes and found lower concentrations of dissolved organic matter in beaches of higher energy. Seidel et al. (2015) conducted an in-depth study on the molecular signatures organic matter that percolated into the beach and proposed that bioavailable carbon compounds of both terrestrial and marine sources stimulated biogeochemical processes, including aerobic respiration, within the cell. More recently, Beck et al. (2017) observed the spatial distribution of solutes, rare earth elements, and genetic material to determine different zones of biogeochemical processes, redox states, and microbial communities within the intertidal circulation cell. Oxygen consumption rates over 1 h for two surficial sediment sampling points were also determined using flow-through columns and air-saturated surface water (Beck et al., 2017). While these studies demonstrate reactivity and reactive potential within the circulation cell, as well as their inferred locations, the depletion of oxygen, the employed proxy for aerobic respiration, is assumed to occur at a constant rate across the beach. A complete spatial distribution of reaction rates that lead to observed solute distributions within the intertidal circulation cell, relative to its salinity distribution, has not been observed.

The present work therefore aims to provide insight into the distribution and magnitudes of aerobic respiration and denitrification rates within the intertidal circulation cell, and their relationship to the salinity distributions and flow regime. We investigated the spatial distribution of reactivity by determining reaction rates using pore water incubation experiments and observing in situ solute concentrations taken from a shore-perpendicular cross section in a tide-dominated sandy beach. Additionally, a numerical variable-density reactive transport model was employed to support the interpretation of field measurements and to provide additional insight into the spatial distribution of reactants and products in the beach aquifer under idealized conditions. The combined results highlight the link between physical processes of flow and the biogeochemical activity within sandy beaches. As sea level rise, beach erosion, or beach remediation efforts alter the slope, width, and hydrogeologic properties of beaches, understanding how the physical flow processes and salinity patterns relate to beach reactivity will become increasingly important.

2. Methods

2.1. Study Site

This study was conducted in the intertidal zone of the tide-dominated Cape Shores beach adjacent to Delaware Bay, near Cape Henlopen, Delaware, USA (Figure 2). Wave action at the Cape Shores site is restricted due to the offshore breakwaters that protect the Lewes Harbor of Refuge. Tides are semidiurnal with an average range of 1.42 m. The beach aquifer is predominantly composed of coarse sand (540–668 μm grain size) and has a hydraulic conductivity of 27.6–30.2 m/d (Heiss et al., 2014).

The biology, chemistry, and hydrology of the intertidal circulation cell at Cape Shores were well characterized in a number of previous studies. Dale and Miller (2007) identified groundwater discharge zones utilizing sediment temperature and pore water salinity distributions along the Cape Shores beach. Active remineralization of organic matter, cycling of N, P, Si, Fe, and S, and seasonal shifts in local microbial communities have also been documented (Dale & Miller, 2008; Hays & Ullman, 2007a, 2007b; McAllister et al., 2015; Miller & Ullman, 2004; Ullman et al., 2003). More recently, Heiss and Michael (2014) investigated the dynamic seasonal movements of the circulation cell in response to changing hydrologic conditions. This makes Cape Shores an ideal site to conduct further research on beach biogeochemistry, as mixing of water masses, active diagenetic cycling of nutrients, and "pulsing" of the cell due to physical forcing have been well documented in the Cape Shores intertidal circulation cell.

2.2. Pore Water Particulate and Solute Analysis

Pore water was collected from seven multilevel samplers along a 30 m beach-perpendicular transect. Each sampler was constructed with multiple polyethylene tubes (7 mm outer diameter) arrayed at 0.5–0.8 m vertical intervals along a PVC support pipe (13 mm outer diameter) extending up to 3 m (Heiss & Michael, 2014). Each polyethylene tube was screened with nylon mesh to prevent clogging. At each location, the sampler was hand augered vertically into the sand (Samplers A–G, Figure 1). A total of 26 sampling ports were distributed within the sampled cross section. Pore water was sampled from the beach during low tide using a peristaltic GeoTech pump, after pumping at least 100 mL to flush out each tube. A YSI Professional Plus meter (Yellow Spring, Ohio) with a flow-through cell was used to measure salinity (practical salinity units), temperature, pH, and redox potential (ORP). An OptiOx Probe (Mettler Toledo, Columbus, Ohio) was used to measure dissolved oxygen (DO) in the field.

Particles in pore water were collected on three precombusted 0.7 μm glass fiber filters, one each for chlorophyll *a*, particulate carbon and nitrogen (PC/PN), and particulate phosphorus (PP), by filtering 1 L of pore water per filter. The filtrate was retained for analysis of dissolved solutes. Chlorophyll was extracted from filters with acetone and quantified using a Turner fluorometer (10 AU; Turner Designs, San Jose California). Pure acetone and standards in acetone provided by Turner were used to calibrate the instrument. The lower detection limit of the fluorometer is 0.025 μg/L. PC/PN was measured by combustion with a Costech CHN Elemental Analyzer with a lower detection limit of 0.005 mg/L. PP was determined spectrometrically, following combustion and acidification using with the molybdenum blue method (Murphy & Riley, 1962).

The 250 mL of the filtrate was preserved in a borosilicate bottle with a greased glass stopper for dissolved inorganic carbon (DIC) and total alkalinity (TA) analysis. These samples were immediately fixed with 80 μl of saturated $HgCl_2$ to prevent further reactions and then stored in the dark at 4°C until analysis. DIC was determined

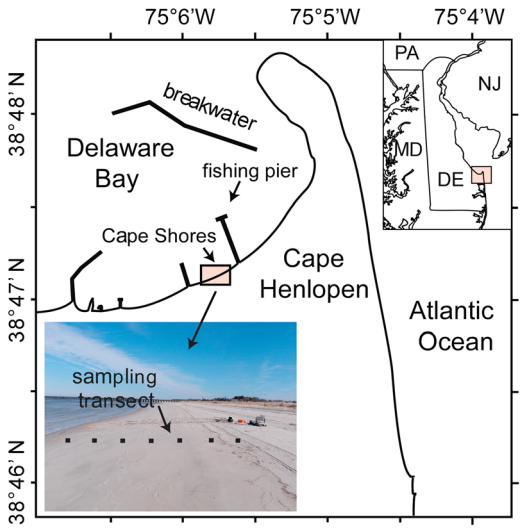

Figure 2. Map of the field site and sampling transect, Cape Shores, Lewes, Delaware, USA.

by acidifying the samples and measuring the evolved CO_2 gas using a Model AS-C3 DIC Analyzer (Apollo SciTech, Newark, Delaware). TA was determined by Gran titration (Gran, 1952) using a Model AS-ALK2 Alkalinity Titrator (Apollo SciTech, Newark, Delaware). Both DIC and TA measurements were calibrated using the certified reference materials from Scripps Institute of Oceanography (San Diego, California). Some samples with high sulfide could not be accurately analyzed for TA due to precipitation of HgS during its fixation with $HgCl_2$. For these samples, DIC and pH measurements were coupled to calculate TA using the Excel macro CO2SYS (Pierrot et al., 2006), with inorganic carbon disassociation constants from Millero et al. (2006). Excess partial pressure of CO_2 (excess pCO_2) was also calculated to observe the effects of aerobic respiration. This was calculated as the difference between in situ DIC and the theoretical DIC value at atmospheric equilibrium (Abril et al., 2000), computed using TA values and atmospheric pCO_2 of 395 μatm (7 September 2014, Mauna Loa Observatory). All measurements of TA, DIC, and pCO_2 were temperature normalized to 15°C to remove thermal effects, leaving only biological and mixing processes. Approximately 100 mL from the remaining filtrate was collected in a Nalgene bottle to measure dissolved nutrients ($NO_2^- + NO_3^-$, NH_4^+, PO_4^{3-}, Si) using standard methods on a SEAL AA3 Autoanalyzer (Mequon, Wisconsin).

Because of sampling limitations due to tide levels, daylight, and sample processing, sampling of all ports could not be completed in 1 day. Preliminary field sampling of a subset of ports, sampled over three consecutive days, found little change in the concentrations and distribution patterns of salinity, temperature, DO, chlorophyll *a*, and PC. This is consistent with prior measurements showing little change in salinity over multiple tidal cycles (Heiss & Michael, 2014). The samples described in this paper were collected on 8 and 10 September 2014.

2.3. Spatial Characterization of Pore Water Reactivity

Unfiltered pore water samples were collected in the field and incubated in the laboratory to determine the spatial patterns of reactivity. Initial O_2 deficit and initial N_2 excess were determined as deviations from the normal atmospheric equilibrium concentrations (NAEC) as a function of salinity and temperature (Garcia & Gordon, 1992; Hamme & Emerson, 2004). O_2 consumption rates and N_2 production rates were determined by incubation. All four parameters were used as indicators of pore water reactivity.

The incubation experiments were similar to those of Kana et al. (1994, 2006). Five unfiltered replicate samples were collected in 12 mL Exetainers with gas-tight caps (Labco, Lampeter Ceredigion, UK) from each sampling port by flooding the test tubes from the bottom end and ensuring no air contamination. The first sample was fixed with 20 μL of saturated $HgCl_2$ at the time of collection in the field to preserve initial in situ measurements of O_2, N_2, and Ar. Initial O_2 deficit and initial N_2 excess was determined from this first aliquot. Some of the first aliquot samples were slightly enriched in O_2 compared to the OptiOx O_2 measurements taken at the time of sampling, most likely due to the short time of exposure to air while the sample was being

Table 1
Reaction Network and Kinetic Rate Expressions (Adopted From Bardini et al. (2012))

Name	Reaction	Rate expression
DOC degradation	$DOC \rightarrow CO_2$	Rate = k_{fox}[DOC];
Aerobic respiration	$DOC + O_2 \rightarrow CO_2 + H_2O$	If $[O_2] >$ kmo2; rate = k_{fox}[DOC]; If $[O_2] <$ kmo2; rate = k_{fox}[DOC] ($[O_2]$/kmo2)
Denitrification	$5DOC + 4NO_3^- + 4H^+ \rightarrow 5CO_2 + 2\,N_2 + 7H_2O$	If $[O_2] >$ kmo2; rate = 0; if $[O_2] <$ kmo2 and $[NO_3^-] >$ kmno3; rate = k_{fox}[DOC] (1 – $[O_2]$/kmo2); If $[O_2] <$ kmo2 and $NO_3^- <$ kmo3; rate = k_{fox}[DOC] (1 – $[O_2]$/kmo2) ($[NO_3^-]$/kno3)

fixed. However, the difference between the two measurements was on average less than 0.5 mg/L, which is similar to the expected uncertainty under flow-through conditions, compounded by instrumentation error (0.5%).

The remaining four aliquoted samples were fixed consecutively over 15 days while being incubated in the dark at 25°C underwater (to minimize gas exchange). No significant amount of additional O_2 was introduced into the samples. Concentrations of O_2 and N_2 relative to the concentration of Ar gas were then measured with high-precision Membrane Inlet Mass Spectrometry (MIMS, PrismaPlus Model; Bay Instruments, Easton, Maryland). The linear regression of O_2 decrease over the first 5 to 7 days of the incubation period was taken as an estimate of the "apparent oxygen consumption rate," related to the oxidation of organic matter at the location of the respective sampling port. Beyond 7 days most samples were anoxic, displayed an air contamination problem, or had a significant change in the rate of apparent O_2 consumption, possibly due to cell growth or exhaustion of more reactive carbon or nutrients. The measured reaction rate was then converted to an "environmental reaction rate" using the Arrhenius equation with an activation energy of 21.5 kcal/mol obtained from the incubation of one Cape Shores sample at three different temperatures (Westrich & Berner, 1988). This activation energy of reaction is similar to those measured in other environmental studies (Aller & Yingst, 1980; Thamdrup et al., 1998). N_2 production rates were determined in a similar manner to O_2 consumption. However, because the MIMS instrument utilized the slope change of O_2/Ar ratios as an indicator of sampling time, it was increasingly difficult to stabilize the instrument for an accurate measurement as samples approached anoxia. For this reason, the interpretation of N_2 increase was approached conservatively.

2.4. Groundwater Flow and Reactive Transport Model

A numerical variable-density groundwater flow and solute transport model was combined with a reactive transport model to simulate tidally driven mixing and biogeochemistry in the beach aquifer. Groundwater flow and conservative salt transport were simulated for a 2-D cross section along the shore-perpendicular transect of multilevel sampling wells using the finite difference code SEAWAT (Langevin et al., 2008). Dissolved organic carbon (DOC) degradation, aerobic respiration, and denitrification along groundwater flow paths was modeled using PHT3D v2.13 (Prommer & Post, 2002). These redox processes were modeled according to the reaction kinetics of DOC, O_2, NO_3^-, N_2 as shown in Table 1 and using the reaction parameter values shown in Table 2. The reactive species were superimposed onto the groundwater flow field simulated using SEAWAT. Thus, the flow and reactive transport simulations were decoupled (Anwar et al. 2014; Bardini et al., 2012; Spiteri et al., 2008).

The model represented an unconfined sandy beach aquifer influenced by tidal and terrestrial freshwater forcing. To avoid boundary effects, the model domain extended 50 m seaward of the mean sea level (MSL)-beachface intersection, 150 m landward, and 30 m below MSL. The beach profile measured prior to the sampling event was set as the top active layer in the model. A nonuniform grid was used to discretize the domain to satisfy Peclet (Pe $<$ 2) and Courant (Cr $<$ 0.75) criteria. Grid

Table 2
Reaction Parameter Values

Parameter and source	Description	Value	Units
k_{fox}[a]	Rate constant for decomposition of DOC	1.5×10^{-6}	s^{-1}
kmo2[a,b]	Limiting concentration of O_2	3.125×10^{-5}	M
kmno3[a,b]	Limiting concentration of NO_3^-	8.065×10^{-6}	M

[a]Van Cappellen and Wang (1996). [b]Bardini et al. (2012).

cells were dx = 0.31 m by dy = 0.06 m in the intertidal zone where rapid flow rates and strong redox gradients occurred. The model was homogenous and isotropic with hydraulic conductivity = 25 m/d, porosity = 0.3, longitudinal dispersivity = 0.15 m, and transverse dispersivity = 0.015. These parameter values were adopted from the calibrated model in Heiss and Michael (2014) for the same sampling transect.

The flow and transport boundary conditions were assigned based on hydrologic forcing and solute concentrations in the fresh and saline groundwater end-members. A constant freshwater flux of 1.01 m^3/d was set along the up-gradient vertical boundary. This flux corresponded to the flux simulated in Heiss and Michael (2014) for the hydraulic head measured at the dune on the 8 September 2014 sampling event at the Cape Shores sampling transect. The influence of tides on flow and transport was simulated with the Periodic Boundary Condition (PBC) Package (Post, 2011). A semidiurnal (period = 0.5 d) sinusoidal tide was assigned using the time-varying head boundary in the PBC package at the shoreface nodes. The tidal amplitude was set to 0.71 m based on the tidal range between mean lower low water (MLLW) and mean higher high water (MHHW) according to the Lewes, DE tide gauge (NOAA tidal station 8557830, Lewes, Delaware) 1 km from the field site. The tidal range between MLLW and MHHW was chosen because it integrates the aquifer conditions over many tidal cycles leading up to the sampling event. Once hydraulic heads and salt concentrations reached dynamic steady state, the tidally averaged fluid fluxes across the shoreface were used to simulate steady state (with respect to boundary conditions) flow and salt transport. The tidally averaged flow field was used to drive the transport of the reactive solutes. The top, bottom, and right boundaries were set as no flow boundaries.

The part of the shoreface where seawater was flowing into the model domain was assigned a source salinity concentration of 28, representing tidally driven seawater infiltration. A zero-concentration gradient for the outflowing portion of the shoreface was set for all species. The end-member concentrations used in the model for DOC, NO_3^-, and O_2 were assigned according to the highest measured values in the end-member source. The end-member concentration for the reactive solutes considered was 66.6 μM for DOC, 179 μM for NO_3^-, and 177 μM for O_2. These end-member concentrations were measured during the sampling event with the exception of DOC, which was measured on 6 November 2014. Seawater flowing into the model domain across the shoreface served as a source of DOC and O_2, and the left vertical boundary served as a source of NO_3^-, representing high-nitrate fresh groundwater flowing into the model domain. DOC and O_2 concentrations in the inflowing fresh groundwater were set to zero, consistent with O_2 measurements and because any reactive DOC in the anoxic environment would have already denitrified a portion of the NO_3^-.

3. Results

3.1. In Situ Pore Water Measurements

Salinity, a nonreactive tracer, outlined the physical location and geometry of the intertidal circulation cell (Figure 3a). Landward of the intertidal zone, a berm was present during sampling period similar to the one observed and described by Heiss and Michael (2014), resulting in some pooling of water as seawater rose above the high tide mark. As a result, a smaller brackish zone was present underneath the depression landward of the berm (Sampler A).

Other chemical parameters showed more spatial variability. pH measurements were circumneutral and ranged from 6.7 to 8.4 (Figure 3b). The most alkaline pH values occurred within the freshwater zones high on the beach. ORP measurements ranged from −77 to +104 mV, with the most oxidizing waters near the fresher zones of Samplers A and B, and intermediate salinity water at Sampler D (Figure 3c). The most reducing conditions were found at the base of the beach near Samplers F and G, where iron and sulfate reduction had been previously observed (McAllister et al., 2015). Overall, ORP patterns did not spatially correlate with salinity. The divergence of chemically sensitive parameters such as pH and ORP from nonreactive parameters like salinity is direct and strong evidence of biogeochemical reactions.

Dissolved oxygen was an important indicator of both water source and beach reactivity. Fresh groundwater in the coastal aquifer below the water table was mostly anoxic, whereas infiltrating saline water was fully oxygenated due to equilibration with the atmosphere. There was a significant decrease in DO (to less than 25% saturation) within the top 2 m of the saline circulation cell, although elevated salinity levels extended to depths of 3 m (Figure 3d). All sampling locations within the beach were undersaturated with respect to

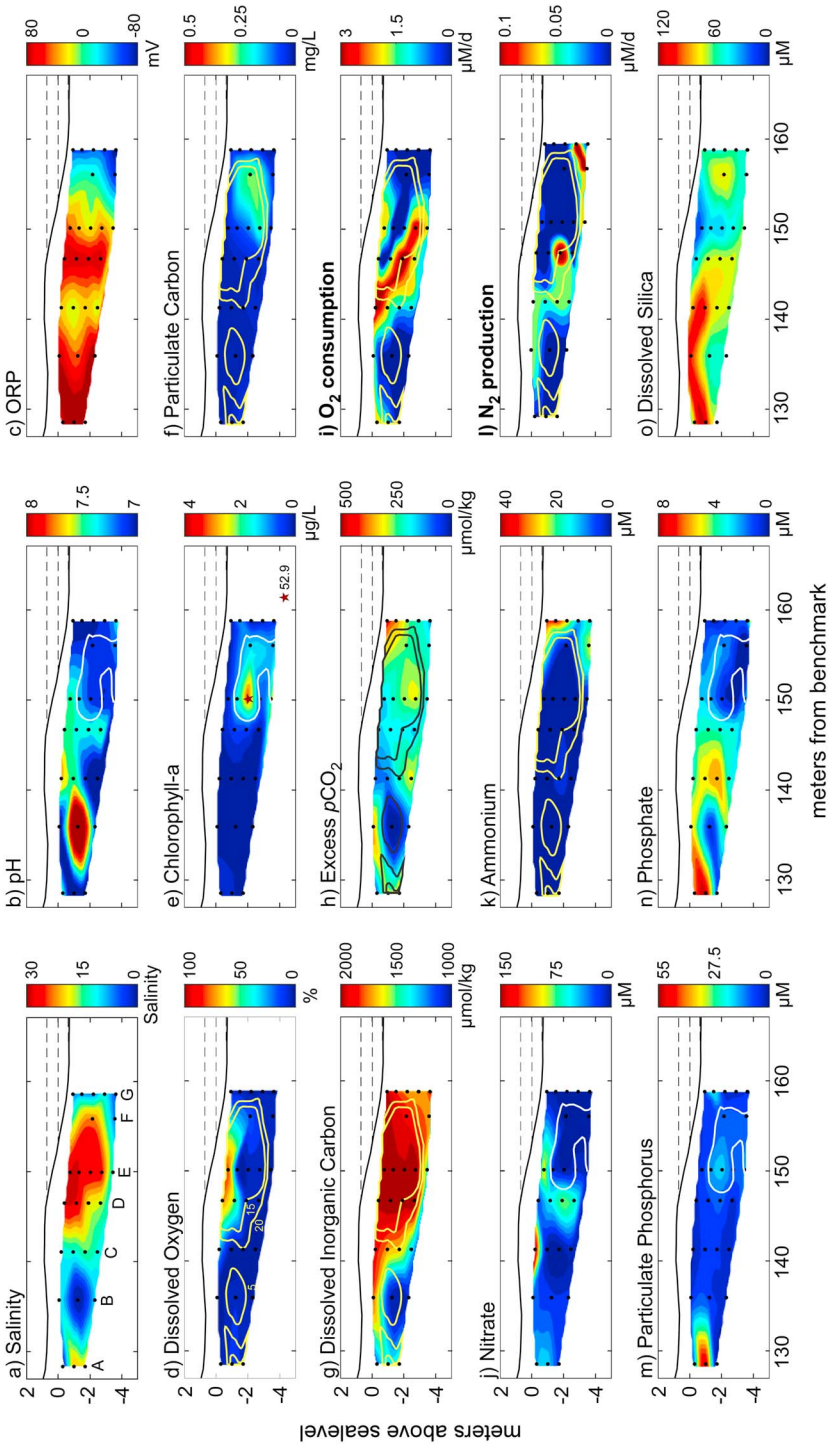

Figure 3. Cross-sectional distributions of measured constituents. Black solid lines delineate surface topography. Dashed lines indicate mean high water, mean sea level, and mean low water (flush with topography). Multilevel pore water samplers are labeled in Figure 3a, with black dots indicating sampling locations. Yellow contours in Figures 3d, 3f–3i, 3k, and 3l (black in Figure 3h) are salinity (5, 15, and 20, labeled in Figure 3d), while white contours (Figures 3b, 3j, 3m, and 3n) show chlorophyll *a* (Figure 3e). Hot spot of chlorophyll is indicated with a star. Figures 3i and 3l (in bold) are from incubation results, while Figures 3a–3h, 3j, 3k, and 3m–3o are in situ measurements or calculations.

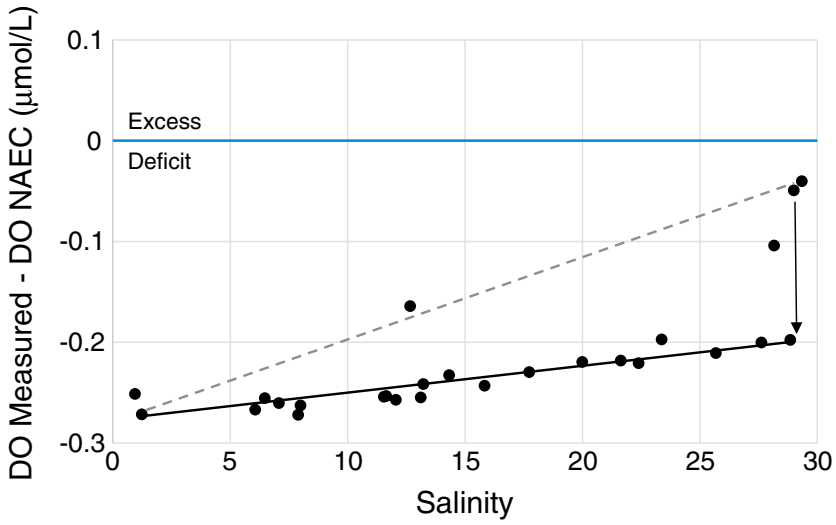

Figure 4. Dissolved oxygen deficit from in situ measurements. All measured DO values are less than the normal atmospheric equilibrium concentration (NAEC) values of DO at its respective salinity and temperature and fall below the zero line (blue solid line). Measurements also all fall below the conservative mixing curve (gray dotted line), except for one sample that was taken from the most landward edge of the intertidal circulation cell at Sampler C. Black vertical arrow highlights rapid depletion of oxygen at high salinities.

atmospheric O_2 (Figure 4) and fell below a salinity-based conservative mixing line between the highest and lowest DO samples (dotted gray line, Figure 4), with the largest deviations at the highest salinities. The observed dilution curve to the lowest salinity sample (solid black line, Figure 4) suggests rapid utilization of oxygen once infiltrated, followed by advective dilution. One exception was the data point on the conservative mixing curve, from the shallowest port on Sampler C where oxygen was still high near the water table at the landward edge of the circulation cell.

Chlorophyll *a*, a proxy for phytoplankton carbon, and particulate carbon (PC) were elevated in the deeper, hypoxic zones of the circulation cell (Figures 3e and 3f). Overall, chlorophyll *a* fluorescence in the subsurface waters of the beach was severely depleted relative to the baywater (~22 µg/L), with 20 ports showing values ranging from 0.0 to 0.9 µg/L. Other than the one hot spot that had 52.9 µg/L (star, Figure 3e), the other five ports had concentrations ranging from 1 to 3 µg/L. PC had a range of 0.01–0.3 mg/L, and the higher values of PC co-occurred with higher chlorophyll concentrations. The filter collected at the high-chlorophyll location was darkly colored with a substantial amount of fine-grained material, suggesting that hydrogeologic conditions at the sampling time allowed for the trapping of finer material in the sampling port. Due to light limitations at this depth (−2.3 m), we do not anticipate in situ phytoplankton growth.

Dissolved inorganic carbon had different spatial patterns compared to particulate organic carbon. Most samples were enriched in DIC relative to the conservative dilution curve, indicating in situ production of CO_2 due to aerobic respiration (Figure 5). Within the aquifer, elevated DIC values mostly coincided with elevated salinity but extended beyond the high-salinity contours (Figure 3g). Because DIC and TA values for both the freshest (1065 µmol/kg, 2066 µmol/kg, respectively) and most saline (1074 µmol/kg, 2048 µmol/kg, respectively) end-member samples were very similar, a fairly conservative 1:1 relationship of TA:DIC with respect to salinity can be assumed. While anaerobic decomposition increases both TA and DIC, aerobic respiration only increases DIC (Cai et al., 2003). Although other minor anaerobic reactions that impact TA:DIC ratios do occur within the aquifer and are important for elemental cycles, such reactions can be overlooked for the purposes of using TA and DIC distributions as evidence of aerobic respiration. Figure 6 shows a relative enrichment of DIC relative to TA above the 1:1 line. Because DIC can be affected by other reactions such as carbonate dissolution or anaerobic processes along the flow path (Cai et al., 2003, 2010; Chaillou et al., 2014, 2016), excess pCO_2 was also calculated as a more direct indicator of aerobic respiration. Save for the lowest salinity sample, all samples had an excess of pCO_2. Consistent with other observations discussed above, the whole intertidal circulation cell displayed high excess pCO_2, with some hot spots within the landward and seaward mixing zones.

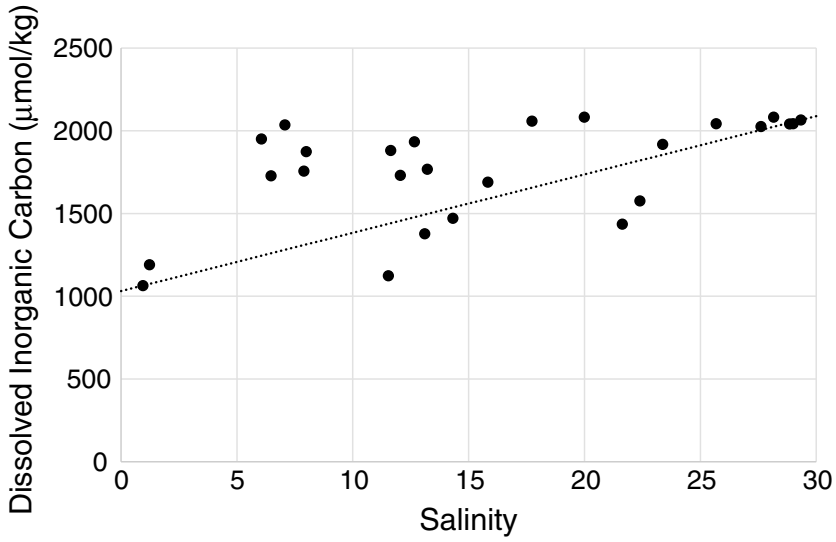

Figure 5. Salinity versus dissolved inorganic carbon. Dotted line indicates conservative mixing curve.

Ammonium and nitrate were spatially separated within the aquifer. Ammonium (~37 μM) was concentrated around Samplers F and G where conditions were much more reducing than the rest of the aquifer and where sulfides were found by McAllister et al. (2015) (Figure 3k). Nitrate, highest around Samplers C and D (~177 μM), was depleted in areas of high ammonium and high particulate organic carbon (Figure 3j). The N_2/Ar ratio measured in the first incubation aliquot at each sampling port, fixed at the time of collection, indicates in situ conditions. N_2/Ar in water in equilibrium with air stays within a remarkably narrow range (36.3–38.5) over a large range of salinities (0–35) and temperatures (5–25) (Weiss, 1970). Yet all samples had a N_2/Ar ratio over 38.5 at intermediate salinities, consistent with microbial N_2 production (not shown).

Particulate phosphorus (PP, Figure 3m) and phosphate (PO_4^{3-}, Figure 3n) were both highest around Sampler A (~55 μM and ~8 μM, respectively) but displayed divergent patterns in other areas of the aquifer. PP concentrations were low overall in the rest of the aquifer, with some elevated concentrations in areas of elevated chlorophyll (pink contour). Phosphate, on the other hand, had a spatial dilution pattern going down gradient from Sampler A and was depleted in the zone of elevated chlorophyll.

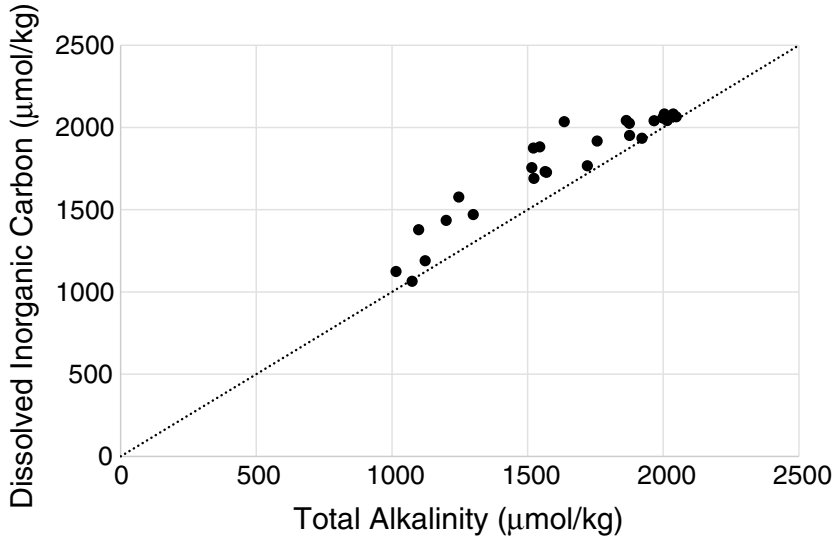

Figure 6. Total alkalinity versus dissolved inorganic carbon, in μmol/kg. Dotted line indicates a 1:1 line.

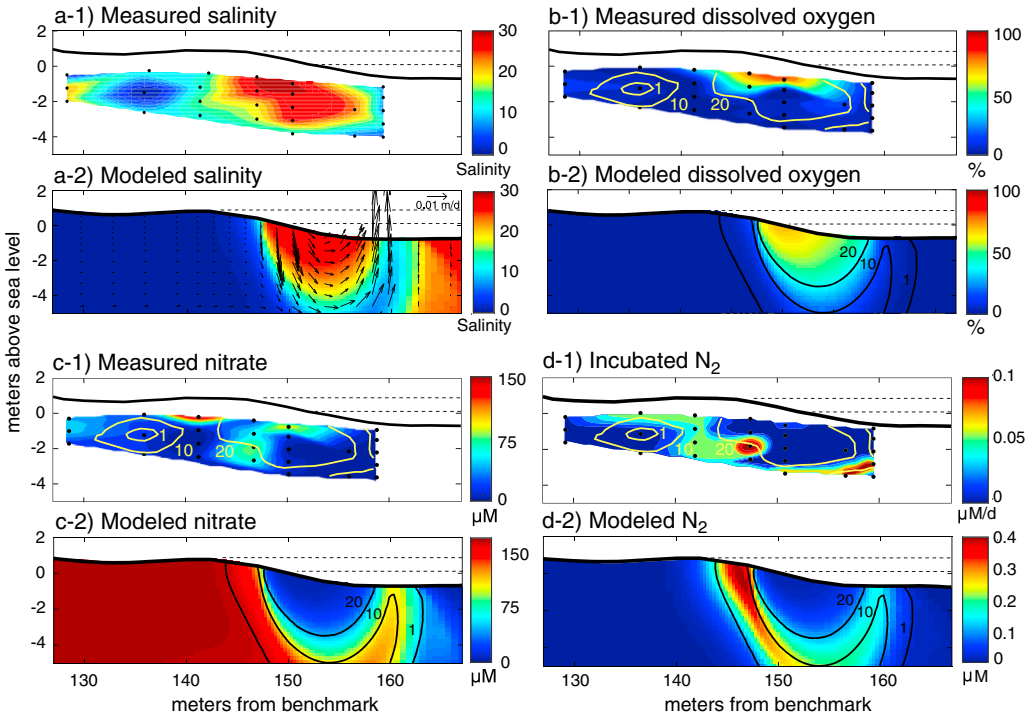

Figure 7. Measured (1) and modeled (2) distributions for (a) salinity, (b) dissolved oxygen, (c) nitrate, and (d) N_2 in the intertidal beach aquifer at Cape Shores, DE. The flow vectors in Figure 7a-2 show the tidally averaged flow direction and magnitude. The horizontal dotted lines in both panels are MHHW and MSL. MLLW is contiguous with the topography at the base of the beachface. The modeled 1, 10, and 20 salinity contours are shown in Figures 7b-2, 7c-2, and 7d-2.

Similar to phosphate, dissolved silica (~123 μM, Figure 3o) was highest at Sampler A and was negatively correlated with salinity, diluting down gradient. There was some apparent production of silica along the flow path, although the highest concentrations did not exceed saturation with respect to amorphous silica by far (~115 μM at 1 atm, 25°C) (Morey et al., 1964).

3.2. Incubation O_2, N_2 Measurements

Aerobic respiration rates from pore water incubations displayed spatial heterogeneity across the beach. Respiration rates ranged from virtually zero to 3 μmol/L/day, with the highest rates along the landward freshwater-seawater (FW-SW) mixing zone in Samplers C and D (Figure 3i).

The measured N_2 gas production rates during incubation was taken as laboratory evidence of denitrification. Because obtaining an accurate gas concentration with MIMS became increasingly difficult as samples became more anoxic, results were interpreted conservatively; only incubations that showed an unequivocal N_2 increase over time were taken to be indicative of denitrification. Samples that did not show an increase in N_2 were assigned a production rate of zero. The highest values of N_2 production were found proximal to the high reactivity zone found in the O_2 incubation experiments, along the landward edges of the circulation cell mixing zone (Figure 3) but also farther along the flow path than hot spots of O_2 consumption in the seaward mixing zone (Figure 3l). This is consistent with expectations that more O_2 consumption would take place near the infiltration point in the circulation cell, while N_2 production would increase toward the end of the flow path near the discharge point.

3.3. Reactive Transport Model Results

The groundwater flow and transport model approximately reproduced the observed salinity distribution in the beach aquifer, the horizontal and vertical extent of the circulation cell, and location of the fresh discharge zone (Figures 7a-1 and 7a-2). Measured and modeled salinities were highest beneath the upper half of the beachface between the MSL-beachface intersection and the high tide mark and decreased with depth and distance seaward due to mixing with underlying fresh groundwater. The upper part of the beach where measured and modeled salinities were highest (X = 150 m) corresponded to the highest rates of seawater

infiltration across the beachface as shown by the magnitude of the flow vectors in Figure 7a-2. The vectors highlight the circulating pattern of saline-brackish groundwater: seawater enters the upper part of the beachface, flows downward and seaward, and then discharges near the base of the beachface (Figure 7a-2). Terrestrially derived fresh groundwater flows seaward beneath the intertidal circulation cell, mixing with saline groundwater along the perimeter of the cell before upwelling at the freshwater discharge zone at the base of the beach.

Measured salinities beneath the backshore landward of the berm ($X \approx 143$ m) were higher than the simulated salinities. This is likely due to the simplifying assumptions of the model, which did not account for temporal variability of seawater input due to spring-neap cycling, seasonality in freshwater flux, storm tides, or waves, all of which can impact salinity and flow patterns in these intertidal systems (Abarca et al., 2013; Boufadel et al., 2007; Heiss & Michael, 2014; C. Robinson et al., 2007; Xin et al., 2010). However, there was good agreement in the location of the fresh discharge zone as well as the spatial coverage of the intertidal mixing zone, key factors related to biogeochemical reactivity and fluxes to the water column.

Measured and modeled dissolved oxygen were highest near the surface below the MSL-beachface intersection where salinity was highest and decreased with depth and distance seaward (Figures 7b-1 and 7b-2). The measured dissolved oxygen saturation decreased more rapidly with depth than the modeled saturation and was higher closer to the surface. The largest discrepancy between measured and modeled nitrate concentrations was in the fresh groundwater (Figures 7c-1 and 7c-2). This can be explained by the modeling choice of a specified flux of nitrate across the entire left boundary, which is consistent with conditions that were generally encountered during sampling during other months of the year, but not in September 2014, highlighting the importance of transient effects. Such transience is caused by precipitation, irregular waves (Xin et al., 2010), spring-neap cycling, seasonality (Heiss & Michael, 2014), as well as variable contaminant loading, and is not captured in the model. Other causes for the deviations between measured and modeled data include lithological and geochemical heterogeneity, or biogeochemical reactions that were not investigated in this study, including iron and sulfate reduction. The discrepancies demonstrate that the biogeochemical framework of these systems is more complex than what can be captured by the present model, even though the general spatial trends are well represented.

Despite the model simplifications, the simulated N_2 results were consistent with the spatial distribution of products and incubation-inferred reactivity in the intertidal aquifer. Modeled N_2 concentrations were elevated in the intertidal mixing zone on the perimeter of the circulation cell and highest below the high tide mark (Figure 7d-2). The model did not reproduce the observed N_2 hot spot 2 m deeper than the highest modeled N_2 concentrations (Figure 7d-1 and 7d-2), and the observed pattern of N_2 is a less well-defined arc than in the model, as expected due to heterogeneity and transience discussed above. However, the patterns of high N_2 production and the high N_2 concentrations are in general agreement. Thus, the model results support the link between the physical flow system and reactivity—the occurrence of denitrification along the outer edge of the intertidal circulation cell that was inferred from the incubation experiments. This consistency supports the interpretation of reactivity derived from incubation experiments and indicates their potential utility in determining the spatial distribution of in situ reactivity in other beach aquifers.

The three independent techniques used in this study to characterize the spatial distribution of denitrification in the Cape Shores beach (N_2/Ar ratio, incubation experiments, and numerical modeling) all indicate that denitrification occurs in the mixing zone on the perimeter of the circulation cell in pore water with salinities ranging between 1 and 20. However, the actual zone of denitrification may be more restricted than the simulated or measured N_2 distribution suggests because of advective-dispersive transport of N_2 outside the active denitrification zone following production.

4. Discussion

It is evident from pH and ORP measurements that biogeochemical reactions are occurring throughout the intertidal circulation cell, as their cross-sectional distributions deviate substantially from the distributions of salinity. Undersaturation with respect to atmospheric O_2 clearly indicates that oxygen consumption occurs in the circulation cell, most likely through aerobic respiration (Figures 3d and 4).

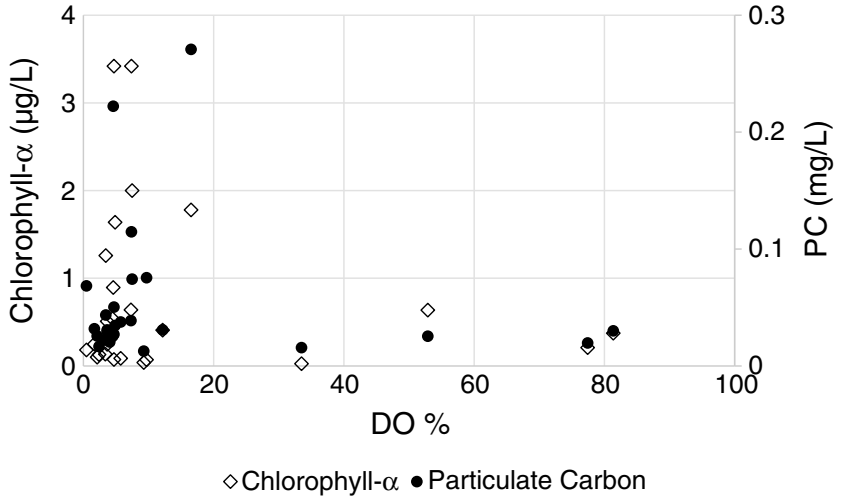

Figure 8. Relationship between chlorophyll and particulate carbon (PC) concentrations, and dissolved oxygen saturation.

However, measured O_2 respiration rates are heterogeneous within the system. They are highest along the landward FW-SW mixing zone where seawater infiltration occurs, supported by in situ measurements of DIC and excess pCO_2, and consistent with CO_2 production during aerobic respiration (Figures 3g–3i). Contrary to our expectations, elevated O_2 consumption rates did not co-occur with higher concentrations of chlorophyll or PC in the pore water. Elevated concentrations of chlorophyll and PC in areas of low in situ DO (Figure 8) suggest that the transformation of these mobile forms of particulate carbon may be oxygen limited, as elevated concentrations are found in the aquifer downstream of the landward mixing zone where oxygen is depleted (Figures 3e, 3f, and 3i). This suggests that a more respirable form of carbon not detected by the methods utilized above may play a larger role in intertidal aquifers than previously expected. Charbonnier et al. (2013) noted that the intertidal beach respiration was at times decoupled from the seasonal phytoplankton bloom and was, most likely, utilizing other sources of bioavailable carbon.

After the rapid consumption of oxygen in the early stages of infiltration, the resulting hypoxic water (<20% saturation) is transported seaward. Within the seaward mixing zone, aerobic respiration occurs at suppressed rates under hypoxic conditions, utilizing less reactive forms of particulate carbon. This is supported by elevated DIC and excess pCO_2 that occur in proximal cross-sectional zones as elevated chlorophyll concentrations (Figures 3e, 3g, and 3h). In addition, Figure 8 shows the oxygen-limited behavior of mobile carbon: the highest concentrations of carbon were observed where DO concentrations were low. This slower respiration of carbon is not expressed in the incubation experiments, presumably because the incubation reaction rates were based on the first 7 days of incubation, when they were linear with time. After 7 days, the experimental reaction rates decreased substantially, perhaps due to a shift to a carbon source with a lower degree of reactivity or changes in the rates of cell growth. Within the beach aquifer, other sedimentary sources of carbon such as microphytobenthos, sediment-entrapped particulate organic carbon (POC), and surface-deposited POC that are not present in pore water incubations could also be supporting respiration (Beck et al., 2017; Charbonnier et al., 2013; Reckhardt et al., 2015). Also, at Cape Shores, on some occasions, beach wrack accumulates with the pooled water behind the berm after very high tides, which may account for the elevated respiration at Sampler A. It is possible that sediment-entrapped particulate carbon not included in pore water incubations, with continuous replenishment of oxygen into the circulation cell during tide and wave action, would allow for respiration rates higher than observed in laboratory incubation experiments.

After aerobic respiration depletes oxygen, denitrification can occur closer to the freshwater discharge point. This is supported by the results of the incubation experiments which show the highest N_2 production rates in the mixing zone (Figure 3l). Reactive transport simulations were consistent with these field and laboratory results and confirm the link between the physical flow system and biogeochemical reactivity. The model demonstrated that nitrogen gas accumulates along circulating flow paths on the perimeter of the circulation cell where saltwater and freshwater mix. The model predicted the highest N_2 concentrations between the 1

and 20 salinity contours, which agrees with the distribution of high N_2 production rates obtained from the incubation experiments (Figure 7b). Because the whole aquifer was enriched in N_2 in situ, there is also a potential for anaerobic ammonium oxidation (anammox) in areas of elevated ammonium (Figure 3k, Samplers F and G). Although oxygen levels in Samplers F and G range from 1 to 13 μM O_2, recent research conducted off the coast of Namibia and Peru by Kalvelage et al. (2011) found anammox to proceed at oxygen levels up to 20 μM, 20 times higher than oxygen levels originally proposed from laboratory cultures of anammox bacteria (Strous et al., 1997). Because the seaward boundary of the intertidal circulation cell experiences frequent shifts in oxygen regimes, it is possible that anaerobic bacteria in this region have adapted to a higher O_2 tolerance.

Other reaction dynamics, such as sorption and dissolution, further affect various solutes within the intertidal circulation cell. High amounts of particulate phosphorus and phosphate are detected near Sampler A, presumably from degradation of the accumulated detritus on the beach surface. PO_4^{3-} then travels downgradient with a dilution pattern but disappears in the region of elevated chlorophyll (Figure 3n, pink contour). Instead, particulate phosphorus is detected in the same region (Figure 3m, pink contour). In addition to P-release during organic matter degradation, phosphate can adsorb readily to particles including the particulate organic matter in this area of the circulation cell (Benitez-Nelson, 2000). When ORP conditions change, this PO_4^{3-} can be released back into the water and become readily available (Föllmi, 1996). The distribution of dissolved silica is related primarily to dilution of freshwater concentrations by seawater, with evidence of production along flow paths, similar to that observed by Charbonnier et al. (2013) (Figure 3o). This may be related to an estuarine source of biogenic silica. Spatial and temporal correlation of dissolved N, P, and Si species are common, due to the similar sources and regeneration patterns, even when regeneration in the case of Si may be related to different processes (Ullman & Welch, 2002; Ullman et al., 2003).

The dominant mechanisms and the extent of biogeochemical reactivity can quickly change in between samplers and within a few weeks in the intertidal circulation cell. High respiration rates along the landward FW-SW mixing zone followed by suppressed rates and denitrification along the seaward FW-SW mixing zone highlight mixing, oxygen availability, and carbon lability as important controls of reactivity at a given location within the intertidal circulation cell. Because dynamic shifts in the geometric shape of the circulation cell alter flow paths, reduction potentials, oxygen and solute concentrations, the understanding of how the biogeochemistry and reactivity relates to its location within the cell is key to the coherent study of this dynamic system.

5. Conclusions

To our knowledge, this work is the first to present independent concentration and reactivity data that describe the relationship between the intertidal circulation cell in beach aquifers and its biogeochemical reactivity (mainly aerobic respiration and denitrification). This complements previous work that postulates reaction locations or redox conditions utilizing solute distributions and supports the conclusion that sandy beaches are important hosts of biogeochemical activity and therefore play important roles in coastal ecology. Based on O_2 consumption and N_2 production rates from incubations, and in situ evidence of excess N_2 and DIC, the highest rates of aerobic respiration and denitrification were found along the FW-SW mixing zone of the intertidal circulation cell. Remineralization of particulate organic carbon is not responsible for the high rates of reaction in this zone but contributes to slower respiration in the seaward FW-SW mixing zone. Numerical simulations show an accumulation of N_2 gas along the 20 salinity contour, consistent with our observations, emphasizing the link between physical and chemical processes. Although the geometry of the intertidal circulation cell will vary by location according to its hydrologic, topographic, and geologic setting, the principle that organic matter consumption is enhanced at the FW-SW mixing zone is likely to endure.

Acknowledgments
We thank Kaileigh Scott, Eric Lunn, Fang Tan, and Mahfuzur Khan for their help in the field. We also thank Matthew Cottrell and Todd Kana for their advice and assistance in operating the MIMS. The authors would also like to acknowledge the two anonymous reviewers for their comments that assisted the improvement of this manuscript. This research was funded by NSF EAR-1246554 (to H. M. and W. J. U.). Data produced in this study are provided in the supporting information (Table S1).

References

Abarca, E., Karam, H., Hemond, H. F., & Harvey, C. F. (2013). Transient groundwater dynamics in a coastal aquifer: The effects of tides, the lunar cycle, and the beach profile. *Water Resources Research*, *49*, 1–16. https://doi.org/10.1002/wrcr.20075

Abril, G., Etcheber, H., Borges, A. V., & Frankignoulle, M. (2000). Excess atmospheric carbon dioxide transported by rivers into the Scheldt estuary. *Comptes Rendus de l'Académie des Sciences - Series IIA - Earth and Planetary Science*, *330*(11), 761–768. https://doi.org/10.1016/S1251-8050(00)00231-7

Aller, R. C., & Yingst, J. Y. (1980). Relationships between microbial distribution and the anaerobic decomposition of organic matter in surface sediments of Long Island Sound, USA. *Marine Biology*, *56*, 29–42. https://doi.org/10.1007/BF00390591

Anschutz, P., Smith, T., Mouret, A., Deborde, J., Bujan, S., Poirer, D., & Lecroart, P. (2009). Tidal sands as biogeochemical reactors. *Estuarine, Coastal and Shelf Science*, *84*, 84–90. https://doi.org/10.1016/j.ecss.2009.06.015

Anwar, N., Robinson, C., & Barry, D. A. (2014). Influence of tides and waves on the fate of nutrients in a nearshore aquifer: Numerical simulations. *Advances in Water Resources*, *73*, 203–213. https://doi.org/10.1016/j.advwatres.2014.08.015

Bakhtyar, R., Brovelli, A., Barry, D. A., Robinson, C., & Li, L. (2013). Transport of variable-density solute plumes in beach aquifers in response to oceanic forcing. *Advances in Water Resources*, *53*, 208–224. https://doi.org/10.1016/j.advwatres.2012.11.009

Bardini, L., Boano, F., Cardenas, M. B., Revelli, R., & Ridolfi, L. (2012). Nutrient cycling in bedform induced hyporheic zones. *Geochimica et Cosmochimica Acta*, *84*, 47–61. http://doi.org/10.1016/j.gca.2012.01.025

Beck, M., Reckhardt, A., Amelsberg, J., Bartholomä, A., Brumsack, H., Cypionka, H., … Zielinski, O. (2017). The drivers of biogeochemistry in beach ecosystems: A cross-shore transect from the dunes to the low water line. *Marine Chemistry*, *190*, 35–50. https://doi.org/10.1016/j.marchem.2017.01.001

Benitez-Nelson, C. (2000). The biogeochemical cycling of phosphorus in marine systems. *Earth-Science Reviews*, *51*(1), 109–135. https://doi.org/10.1016/S0012-8252(00)00018-0

Boudreau, B. P., Huettel, M., Forster, S., Jahnke, R. A., McLachlan, A., Middelburg, J. J., … Sundby, B. (2001). Permeable marine sediments: Overturning an old paradigm. *EOS Transactions American Geophysical Union*, *82*(11), 133–136. https://doi.org/10.1029/EO082i011p00133-01

Boufadel, M. C., Li, H., Suidan, M. T., & Venosa, A. D. (2007). Tracer studies in a laboratory beach subjected to waves. *Journal of Environmental Engineering*, *133*, 722–732. https://doi.org/10.1061/(ASCE)0733-9372(2007)133:7(722)

Burnett, W. C., Bokuniewicz, H., Huettel, M., Moore, W. S., & Taniguchi, M. (2003). Groundwater and pore water inputs to the coastal zone. *Biogeochemistry*, *66*(1/2), 3–33. https://doi.org/10.1023/B:BIOG.0000006066.21240.53

Cai, W. J., Wang, Y., Krest, J., & Moore, W. S. (2003). The geochemistry of dissolved inorganic carbon in a surficial groundwater aquifer in North Inlet, South Carolina, and the carbon fluxes to the coastal ocean. *Geochimica et Cosmochimica Acta*, *67*(4), 631–639. https://doi.org/10.1016/S0016-7037(02)01167-5

Cai, W. J., Luther, G. W., Cornwell, J. C., & Giblin, A. E. (2010). Carbon cycling and the coupling between proton and electron transfer reactions in aquatic sediments in Lake Champlain. *Aquatic Geochemistry*, *16*(3), 421–446. https://doi.org/10.1007/s10498-010-9097-9

Chaillou, G., Couturier, M., Tommi-Morin, G., & Rao, A. M. (2014). Total alkalinity and dissolved inorganic carbon production in groundwaters discharging through a sandy beach. *Procedia Earth and Planetary Science*, *10*, 88–99. https://doi.org/10.1016/j.proeps.2014.08.017

Chaillou, G., Lemay-Borduas, F., & Couturier, M. (2016). Transport and transformations of groundwater-borne carbon discharging through a sandy beach to a coastal ocean. *Canadian Water Resources Journal*, *41*(4), 455–468. https://doi.org/10.1080/07011784.2015.1111775

Charbonnier, C., Anschutz, P., Poirier, D., Bujan, S., & Lecroart, P. (2013). Aerobic respiration in a high-energy sandy beach. *Marine Chemistry*, *155*, 10–21. https://doi.org/10.1016/j.marchem.2013.05.003

Charette, M. A., & Sholkovitz, E. R. (2002). Oxidative precipitation of groundwater-derived ferrous iron in the subterranean estuary of a coastal bay, *Geophysical Research Letters*, *29*(10), 1444. https://doi.org/10.1029/2001GL014512

Cooper, H. H., Jr. (1959). A hypothesis concerning the dynamic balance of fresh water and salt water in a coastal aquifer. *Journal of Geophysical Research*, *64*(4), 461–467. https://doi.org/10.1029/JZ064i004p00461

Dale, R. K., & Miller, D. C. (2007). Spatial and temporal patterns of salinity and temperature at an intertidal groundwater seep. *Estuarine, Coastal and Shelf Science*, *72*(1), 283–298. https://doi.org/10.1016/j.ecss.2006.10.024

Dale, R. K., & Miller, D. C. (2008). Hydrologic interactions of infaunal polychaetes and intertidal groundwater discharge. *Marine Ecology Progress Series*, *363*, 205–215. https://doi.org/10.3354/meps07455

Föllmi, K. B. (1996). The phosphorus cycle, phosphogenesis and marine phosphate-rich deposits. *Earth-Science Reviews*, *40*(1–2). https://doi.org/10.1016/0012-8252(95)00049-6

Garcia, H. E., & Gordon, L. I. (1992). Oxygen solubility in seawater: Better fitting equations. *Limnology and Oceanography*, *37*, 1307–1312. (and erratum 38, 656), https://doi.org/10.4319/lo.1992.37.6.1307

Gran, G. (1952). Determination of the equivalence point in potentiometric titrations, Part II. *Analyst*, *77*(920), 661–671. https://doi.org/10.1039/an9527700661

Hamme, R. C., & Emerson, S. R. (2004). The solubility of neon, nitrogen, and argon in distilled water and seawater. *Deep-Sea Research*, *51*, 1517–1528. https://doi.org/10.1016/j.dsr.2004.06.009

Hays, R. L., & Ullman, W. J. (2007a). Direct determination of total and fresh groundwater discharge and nutrient loads from a sandy beachface at low tide (Cape Henlopen, Delaware). *Limnology and Oceanography*, *52*(1), 240–247. https://doi.org/10.4319/lo.2007.52.1.0240

Hays, R. L., & Ullman, W. J. (2007b). Dissolved nutrient fluxes through a sandy estuarine beachface (Cape Henlopen, Delaware, USA): Contributions from fresh groundwater discharge, seawater recycling, and diagenesis. *Estuaries and Coasts*, *30*(4), 710–724. https://doi.org/10.1007/BF02841967

Heiss, J. W., & Michael, H. A. (2014). Saltwater-freshwater mixing dynamics in a sandy beach aquifer over tidal, spring-neap, and seasonal cycles. *Water Resources Research*, *50*, 6747–6766. https://doi.org/10.1002/2014WR015574

Heiss, J. W., Ullman, W. J., & Michael, H. A. (2014). Swash zone moisture dynamics and unsaturated infiltration in two sandy beach aquifers. *Estuarine, Coastal and Shelf Science*, *143*, 20–31. https://doi.org/10.1016/j.ecss.2014.03.015

Johannes, R. E. (1980). Ecological significance of the submarine discharge of groundwater. *Marine Ecology Progress Series*, *3*(4), 365–373.

Kalvelage, T., Jensen, M. M., Contreras, S., Revsbech, N. P., Lam, P., Günter, M., … Kuypers, M. M. (2011). Oxygen sensitivity of anammox and coupled N-cycle processes in oxygen minimum zones. *PloS One*, *6*(12), e29299. https://doi.org/10.1371/journal.pone.0029299

Kana, T. M., Darkangelo, C., Duane Hunt, M., Oldham, J. B., Bennett, G. E., & Cornwell, J. C. (1994). Membrane inlet mass spectrometer for rapid high-precision determination of N_2, O_2, and Ar in environmental water samples. *Analytical Chemistry*, *66*, 4166–4166. https://doi.org/10.1021/ac00095a009

Kana, T. M., Cornwell, J. C., & Zhong, L. (2006). Determination of denitrification in the Chesapeake Bay from measurements of N_2 accumulation in bottom water. *Estuaries and Coasts*, *29*(2), 222–231. https://doi.org/10.1007/BF02781991

Kohout, F. A. (1960). Cyclic flow of salt water in the Biscayne aquifer of southeastern Florida. *Journal of Geophysical Research*, *65*(7), 2133–2141. https://doi.org/10.1029/JZ065i007p02133

Langevin, C. D., Thorne, D. T., Jr., Dausman, A. M., Sukop, M. C., & Guo, W. (2008). SEAWAT version 4: A computer program for simulation of multi-species solute and heat transport, No. 6–A22. Geological Survey (US).

McAllister, S. M., Barnett, J. M., Heiss, J. W., Findlay, A. J., MacDonald, D. J., Dow, C. L., … Chan, C. S. (2015). Dynamic hydrologic and biogeochemical processes drive microbially enhanced iron and sulfur cycling within the intertidal mixing zone of a beach aquifer. *Limnology and Oceanography*, *60*, 329–345. https://doi.org/10.1111/lno.10029

Michael, H. A., Mulligan, A. E., & Harvey, C. F. (2005). Seasonal oscillations in water exchange between aquifers and the coastal ocean. *Nature*, *436*(7054), 1145–1148. https://doi.org/10.1038/nature03935

Miller, D. C., & Ullman, W. J. (2004). Ecological consequences of ground water discharge to Delaware Bay, United States. *Ground Water*, *42*(7), 959–970. https://doi.org/10.1111/j.1745-6584.2004.tb02635.x

Millero, F. J., Graham, T. B., Huang, F., Bustos-Serrano, H., & Pierrot, D. (2006). Dissociation constants of carbonic acid in seawater as a function of salinity and temperature. *Marine Chemistry*, *100*, 80–94. https://doi.org/10.1016/j.marchem.2005.12.001

Moore, W. S. (1999). The subterranean estuary: A reaction zone of ground water and sea water. *Marine Chemistry*, *65*(1), 111–125. https://doi.org/10.1016/S0304-4203(99)00014-6

Morey, G. W., Fournier, R. O., & Rowe, J. J. (1964). The solubility of amorphous silica at 25 °C. *Journal of Geophysical Research*, *69*(10), 1995–2002. https://doi.org/10.1029/JZ069i010p01995

Murphy, J. R., & Riley, J. P. (1962). A modified single solution method for the determination of phosphate in natural waters. *Analytica Chimica Acta*, *27*, 31–36. https://doi.org/10.1016/S0003-2670(00)88444-5

Pierrot, D., Lewis, E., & Wallace, D. W. R. (2006). CO2SYS DOS program developed for CO2System calculations. In *ORNL/CDIAC-105, carbon dioxide information analysis center*. Oak Ridge, TN: Oak Ridge National Laboratory, US Department of Energy.

Post, V. E. A. (2011). A new package for simulating periodic boundary conditions in MODFLOW and SEAWAT. *Computers and Geosciences*, *37*(11), 1843–1849. https://doi.org/10.1016/j.cageo.2011.01.012

Prommer, H., & Post, V. (2002). A reactive multicomponent transport model for saturated porous media, *User's manual version* 1, 141.

Reckhardt, A., Beck, M., Seidel, M., Riedel, T., Wehrmann, A., Bartholomä, A., & Brumsack, H. J. (2015). Carbon, nutrient and trace metal cycling in sandy sediments: A comparison of high-energy and backbarrier tidal flats. *Estuarine, Coastal and Shelf Science*, *159*, 1–14. https://doi.org/10.1016/j.ecss.2015.03.025

Robinson, C., Gibbes, B., & Li, L. (2006). Driving mechanisms for groundwater flow and salt transport in a subterranean estuary. *Geophysical Research Letters*, *33*, L03402. https://doi.org/10.1029/2005GL025247

Robinson, C., Gibbes, B., Carey, H., & Li, L. (2007). Salt-freshwater dynamics in a subterranean estuary over a spring-neap tidal cycle. *Journal of Geophysical Research*, *112*, C09007. https://doi.org/10.1029/2006JC003888

Robinson, M., Gallagher, D., & Reay, W. (1998). Field observations of tidal and seasonal variations in ground water discharge to tidal estuarine surface water. *Groundwater Monitoring & Remediation*, *18*(1), 83–92. https://doi.org/10.1111/j.1745-6592.1998.tb00605.x

Seidel, M., Beck, M., Greskowiak, J., Riedel, T., Waska, H., Suryaputra, I. G. N. A., … Dittmar, T. (2015). Benthic-pelagic coupling of nutrients and dissolved organic matter composition in an intertidal sandy beach. *Marine Chemistry*, *176*, 150–163. https://doi.org/10.1016/j.marchem.2015.08.011

Slomp, C. P., & Van Cappellen, P. (2004). Nutrient inputs to the coastal ocean through submarine groundwater discharge: Controls and potential impact. *Journal of Hydrology*, *295*(1), 64–86. https://doi.org/10.1016/j.jhydrol.2004.02.018

Spiteri, C., Slomp, C. P., Tuncay, K., & Meile, C. (2008). Modeling biogeochemical processes in subterranean estuaries: Effect of flow dynamics and redox conditions on submarine groundwater discharge of nutrients. *Water Resources Research*, *44*, W02430. https://doi.org/10.1029/2007WR006071

Strous, M., Van Gerven, E., Kuenen, J. G., & Jetten, M. (1997). Effects of aerobic and microaerobic conditions on anaerobic ammonium-oxidizing (anammox) sludge. *Applied and Environmental Microbiology*, *63*(6), 2446–2448.

Thamdrup, B., Hansen, J. W., & Jorgensen, B. B. (1998). Temperature dependence of aerobic respiration in a coastal sediment. *FEMS Microbiology Ecology*, *25*(2), 189–200. https://doi.org/10.1111/j.1574-6941.1998.tb00472.x

Ullman, W. J., & Welch, S. A. (2002). Organic ligands and feldspar dissolution. In R. Hellmann, & S. A. Wood (Eds.), *Water-rock interactions, ore deposits, and environmental geochemistry: A tribute to David Crerar., special publication 7* (pp. 3–35). St. Louis, MO: The Geochemical Society.

Ullman, W. J., Chang, B., Miller, D. C., & Madsen, J. A. (2003). Groundwater mixing, nutrient diagenesis, and discharges across a sandy beachface, Cape Henlopen, Delaware (USA). *Estuarine, Coastal and Shelf Science*, *57*(3), 539–552. https://doi.org/10.1016/S0272-7714(02)00398-0

Van Cappellen, P., & Wang, Y. (1996). Cycling of iron and manganese in surface sediments: A general theory for the coupled transport and reaction of carbon, oxygen, nitrogen, sulfur, iron, and manganese. *American Journal of Science*, *296*(3), 197–243. https://doi.org/10.2475/ajs.296.3.197

Weiss, R. F. (1970). The solubility of nitrogen, oxygen and argon in water and seawater. *Deep Sea Research and Oceanographic Abstracts*, *17*(4), 721–735. https://doi.org/10.1016/0011-7471(70)90037-9

Westrich, J. T., & Berner, R. A. (1988). The effect of temperature on rates of sulfate reduction in marine sediments. *Geomicrobiology Journal*, *6*, 99–117. https://doi.org/10.1080/01490458809377828

Xin, P., Robinson, C., Li, L., Barry, D. A., & Bakhtyar, R. (2010). Effects of wave forcing on a subterranean estuary. *Water Resources Research*, *46*, W12505. https://doi.org/10.1029/2010WR009632